THE JOURNAL OF PHYSICAL CHEMISTRY Letters

Letter

Cite This: J. Phys. Chem. Lett. 2019, 10, 6316−6323

pubs.acs.org/JPCL

Phase Diagram of Nanoscale Water on Solid Surfaces with Various Wettabilities

Hu Qiu* and Wanlin Guo*

State Key Laboratory of Mechanics and Control of Mechanical Structures and Key Laboratory for Intelligent Nano Materials and Devices of MOE, Institute of Nano Science, Nanjing University of Aeronautics and Astronautics, Nanjing 210016, China

Supporting Information

ABSTRACT: Understanding structural and dynamic properties of water in contact with solid surfaces is essential for diverse fields, including environmental sciences, nanofluidics, lubrication, and electrochemistry. Despite tremendous efforts, how interfacial water phase behaviors correlate with a surface's wettability remains elusive. Here, we investigate the structure and dynamics of nanoscale water droplets or adlayers on solid surfaces with wettabilities spanning from strongly hydrophobic to strongly hydrophilic using extensive molecular dynamics simulations. It is shown that liquid water drops on solid surfaces with contact angles greater than 42.6° transform into drops of ordinary hexagonal ice (I_h) upon cooling. In contrast, water forms a liquid disc on a completely wetted surface with a zero contact angle, which freezes into a hexagonal bilayer ice disc at low temperatures. Unexpectedly, on surfaces with a mild contact angle in the range of 21.9°−29.2°, the originally stable liquid drop at room temperature further wets the surface upon cooling and eventually transforms into a bilayer ice disc. These results establish a phase diagram of nanoscale water at the wettability versus temperature plane, which may expand our knowledge of water−surface interactions as well as enrich the complexity of water behaviors at interfaces.

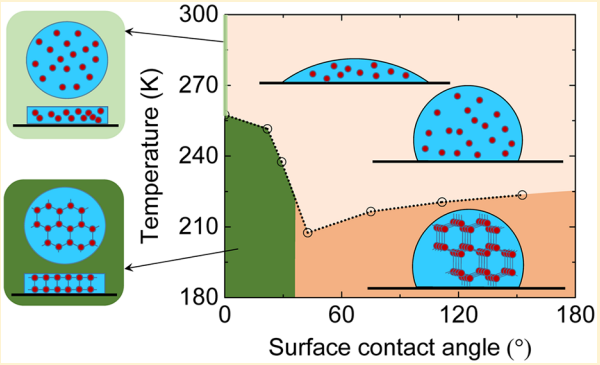

Water−surface interactions are ubiquitous in nature and relevant to a broad range of processes such as catalysis, protein folding, lubrication, and aqueous electrochemistry. In protein folding, for example, the interaction of a protein with the surrounding water mediates the collapse of the protein chain and drives the search for the native protein structure through a funneled energy landscape.[1] To elucidate how water behaves at interfaces, numerous experiments and simulations have been performed on surfaces with various structural and chemical characteristics (e.g., metal,[2] metal oxide,[3] self-assembled monolayers,[4,5] mica,[6] and graphene[7−9]). In particular, molecular-level understanding of water−solid interfaces has been acquired through a few surface-science-style experiments on flat metal substrates, which operate usually in ultrahigh vacuum conditions at cryogenic temperatures (up to about 200 K).[2,10] A variety of structures for adsorbed water (usually at the nanoscale), including water clusters,[11] one-dimensional ice chains,[12] and extended water overlayers,[13] have been visualized on metal surfaces such as Cu(111), Cu(110), and Pt(111). In particular, a bilayer ice crystalline was observed in experiments on graphene coated Pt(111),[14] which consisted of two flat hexagonal sheets of water molecules; a similar ice phase was predicted in molecular dynamics (MD) simulations for water confined between two planar smooth walls.[15−17] In addition to structures, the properties of water molecules binding strongly to surfaces may also vary with respect to those of bulk ones. For instance, a water monolayer on a Pt(111) surface did not allow for the further wetting of subsequent layers at extremely low temperatures, yielding a so-called hydrophobic ice layer.[18] Likewise, two-dimensional hydrophobic-like water/ice layers were observed at room temperature in simulations on ionic surfaces with a specific pattern of charge distribution[19,20] and in experiments confined between graphene and MoS_2.[21]

It is known that the structures and properties of interfacial water are closely related to the properties of surfaces. Among these properties is the surface wettability, which depends on the chemical composition and geometric structure of surfaces. The surface wettability is generally quantified by measuring the contact angle θ at the solid−liquid interface; when θ is above 90°, the surface is considered to be hydrophobic, and when θ is below 90°, the surface is considered to be hydrophilic. Expectedly, the microscopic structures and properties of water in the vicinity of a hydrophobic surface differ from those near a hydrophilic surface, such as fluctuation in local density, water−water correlation, and the probability of cavity formation.[4] The consequence of these differences is the distinct macroscopic behaviors of water near hydrophobic and hydrophilic surfaces. In this regard, a representative example is

Received: August 27, 2019
Accepted: September 30, 2019
Published: September 30, 2019

DOI: 10.1021/acs.jpclett.9b02512
J. Phys. Chem. Lett. 2019, 10, 6316−6323

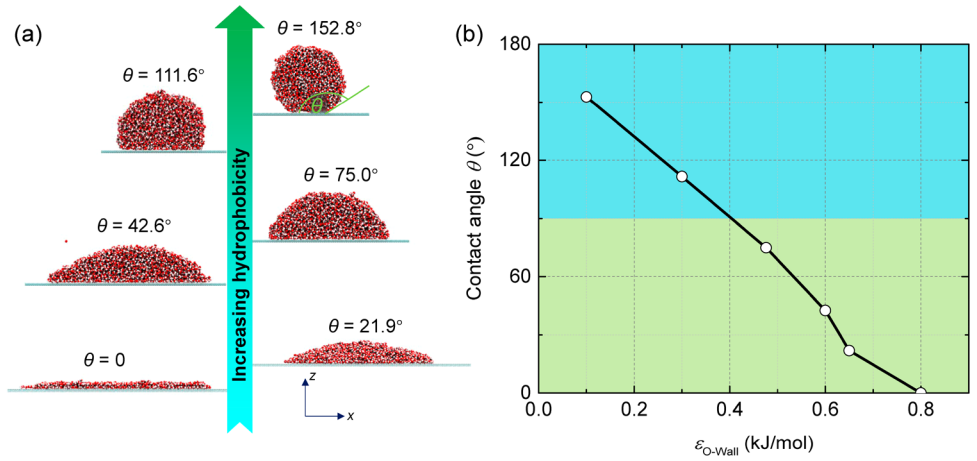

Figure 1. (a) Relaxed configuration of nanoscale water on model solid surfaces with various wettabilities. The determined macroscopic contact angle θ, i.e. the contact angle corresponding to an infinitely large droplet (see Models and Methods), is labeled to characterize surface wettability. (b) Contact angle θ as a function of the water−surface interaction parameter ε_{O-Wall}.

the freezing behavior of interfacial water. Ice nucleation on a hydrophilic surface was found to be about one order of magnitude faster than that on a hydrophobic flat surface.[22] Indeed, water wetting on hydrophobic surfaces at ambient conditions, unlike hydrophilic surfaces, is not favorable such that the molecular level observation of ice formation on these surfaces is a challenging task. By introducing hydrophilic graphene oxide nanoflakes (nanoGO) as the seed for ice nucleation on a hydrophobic graphite surface, Zheng et al. reported dynamic processes involved in room-temperature ice formation of one-dimensional ice chain and three-dimensional ice (I_c and I_h), depending on the coverage of nanoGO and humidity levels.[23] Recently, Liu et al. provided new insights into the influence of wettability on ice growth and found two distinct ice growth modes on solid surfaces with different wettabilities: along-surface and off-surface growth modes.[24] The former mode was attributed to the presence of a bilayer ice on hydrophilic surfaces, which shares a similar structural feature with hexagonal bulk ice (I_h) and thus promotes the along-surface growth of I_h ice as a result of the lattice match. A few other investigations have also been carried out to study ice formation on surfaces with different wettabilities, mostly from a macroscopic point-of-view.[25,26] Despite much progress, a comprehensive picture of microscopic water structures and phase transition behaviors on surfaces spanning over a wide range of wettabilities (i.e., the phase diagram) has not been established.

Here we investigate structure and dynamics of nanometer-sized liquid water droplets and adlayers and associated freezing processes during cooling on model surfaces with various wettabilities. Different morphologies of nanoscale liquid water, such as drops of bulklike water in different shapes and ultrathin discs containing bilayer water, are as expected present at 300 K depending on surface wettabilities. These water structures transform into corresponding ice phases upon cooling. We characterize the freezing transition temperature as well as the structure and dynamics of each nanoscale water/ice phase and eventually propose a schematic phase diagram at the wettability−temperature plane.

In the present work, we considered a series of model surfaces with a broad range of wettabilities (Figure 1a); the water contact angle θ is in the range of 0−152.8°, which was realized by adjusting the water−surface interaction parameter ε_{O-Wall} (Figure 1b). The protocol used to measure θ is provided in Figure S1 and Models and Methods. In a typical phase behavior simulation, a droplet of TIP4P/2005 water[27] was placed in contact with each model surface, followed by a system relaxation for 50 ns at ambient temperature (T = 300 K). Subsequently, each system was cooled gradually, with a temperature interval of 10 K (except for simulations around the freezing point where the temperature interval was reduced to 1 K), during which the phase behavior was traced by examining interfacial water's diffusivity, density distribution, etc. The length of these simulations ranged from 50 ns to 2.1 μs, depending on the surface wettability and temperature.

We first considered a hydrophobic surface with a contact angle θ at 111.6° and monitored water diffusion coefficient D of a water droplet on this surface when the temperature was decreased from 300 to 200 K, as shown in Figure 2a (empty squares). The decrease in D upon cooling indicates a gradually reduced water mobility. However, no evidence of freezing (or crystallization) transition was seen after visual inspection of the simulation trajectories at temperatures as low as 200 K, although the melting point of bulk ice I_h described with the TIP4P/2005 water model was reported to be around 250.5 K.[28] This is not a surprising observation, as the limited time scale of MD simulations may not allow for the homogeneous seed nucleation of ice. To promote freezing of the drop, a so-called direct coexistence technique[28] was used in simulations below 250 K. Specifically, after system relaxation at each temperature, some water molecules around the center of the supercooled water drop were replaced by a sphere of ice I_h, which acted as the ice nuclei to promote possible crystallization (see Figure S2a and Models and Methods for detailed descriptions). The resulting system was further equilibrated for ∼500 ns in order to study the freezing and melting of the drop. At temperatures above 221 K, the decreasing number of water molecules constituting the ice crystal in the drop indicates the melting of the system, whereas at temperatures below 220 K, this number increases, manifesting the freezing of the drop (top right panel in Figure S2). The resulting freezing/melting temperature, calculated approximately as the middle point between the above two temperatures, is 220.5 K. Meanwhile, the calculated diffusion coefficients for systems that were successfully frozen (namely, below 220 K), shown as filled squares in Figure 2a, are several-

DOI: 10.1021/acs.jpclett.9b02512
J. Phys. Chem. Lett. 2019, 10, 6316−6323

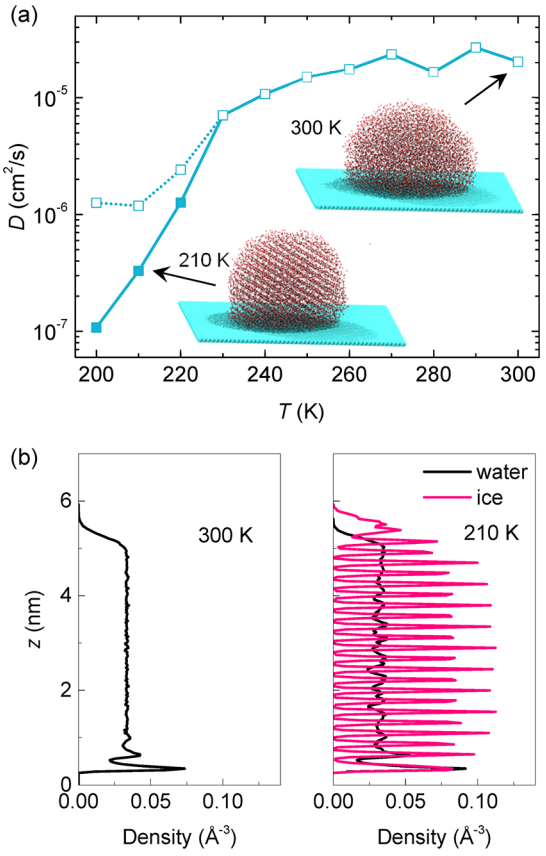

Figure 2. Freezing of a water drop on a hydrophobic surface with a contact angle of 111.6°. (a) Diffusion coefficient of water D as a function of gradually decreasing temperature T. At T below 250 K, the water drop was first equilibrated (empty squares), and then a spherical ice seed (I_h) was introduced to the equilibrated water droplet to promote freezing. Successful freezing of the drop occurred at T less than ~220 K, as indicated by reduced diffusion coefficients (filled squares). Insets show snapshots of a liquid water drop at 300 K and an ice drop at 210 K. (b) Transverse density profiles of water oxygen atoms normal to the surface at 300 K (left) and 210 K (right). At 210 K, water densities of the drop in a liquidlike form (before crystallization; black line) and a solid form (after crystallization; red line) are both shown. Water molecules within a 0.5 nm radius cylinder with its axis centered at the center of mass of the drop and normal to the surface were considered in density calculation. Note that the exact density profile of the drop in the solid form may vary depending on its orientation.

fold lower than those in a supercooled liquidlike phase at the same temperatures (empty squares). This difference proves the reduced mobility of water molecules in an ice phase compared to a liquidlike phase. In addition, the instantaneous snapshot of the nanodrop indicates a disordered liquid water phase (top inset in Figure 2a), whereas an ordered solid phase is present after freezing at low temperatures (bottom inset in Figure 2a). It is noteworthy that the diffusion coefficients for the ice phase are still relatively high (compared to that for bulk ice), likely because of the presence of mobile liquid water layers near the surface of ice drops. Such a liquidlike layer is ubiquitous on ice surfaces at temperatures below the melting point, the so-called surface premelting of ice.[29]

The freezing transition occurring in the nanodrop can be further validated by comparing the transverse density distribution of water oxygen atoms (normal to the surface) in different phases. In the liquid phase at 300 K (left panel in Figure 2b), density fluctuation (i.e., layering) is seen only nearest to the water−solid interface with z less than 1.2 nm, and when z is above 1.2 nm, the flat density curve confirms that the liquid water is unstructured. Likewise, the supercooled drop before crystallization also exhibits a slight density fluctuation distant from the interfacial region (black curve in the right panel of Figure 2b). In contrast, the oxygen density profile for the ice phase after crystallization exhibits pronounced peaks (red curve), confirming the presence of well-defined oxygen layers inside the ice drop.

When the surface is switched to a more hydrophilic one with smaller θ (75.0° or 42.6°) or a more hydrophobic one with larger θ (152.8°), the overall shape of the liquid water drops vary as expected (see Figure 1). Nevertheless, the freezing transition process upon cooling is analogous to the picture depicted above, albeit at slightly different crystallization temperatures determined using the direct coexistence technique (Figure S2b). Likewise, spontaneous crystallization has been reported for a droplet of mW (i.e., a coarse-grained water model) water on graphite surfaces with a contact angle of 86°.[30] Note that no seed nuclei was used therein, presumably because of the use of different water models.

We next focus on a surface with the "ultimate" hydrophilicity, namely a completely wetted surface with $\theta = 0$. At first glance, a gradual decrease in lateral diffusion coefficient D_{xy} emerges versus decreasing T (filled squares in Figure 3a), in qualitative accord with that on the above surfaces without complete wetting. However, visual inspection of the simulation trajectory suggests that a nanoscale disc (nanodisc) containing two layers of water molecules is present at 300 K on this superhydrophilic surface (top panel in Figure 3b). Upon cooling, D_{xy} drops suddenly in the temperature range between 258 and 257 K (Figure 3a), yielding the freezing/melting point at 257.5 K. Below 257 K, the system transforms into a bilayer ice phase (bottom panel in Figure 3b). Note that this ice phase consists of two hexagonal planar layers in registry with each other (namely, atoms from each layer are placed directly on top of each other). It closely resembles the bilayer ice usually predicted between two parallel walls (namely, under nanoconfinement), based on the two following observations. On one hand, its lattice constant is approximately 0.482 nm, comparable to that of confined bilayer ice phases in previous ab initio MD simulations at 0.476 nm.[14] Besides, the two oxygen planes are separated by 0.280 nm (as discussed below), again consistent with previous results[14] (0.285 nm). On the other hand, the freezing transition into the bilayer ice in both the present work and previous simulation studies[15,16] is a spontaneous process, that is, without the need of a ice nuclei used in the above nanodrop freezing simulations. It is noteworthy that experimental evidence of such a hexagonal two-layer structure has been available for water confined between graphene and MoS_2 at room temperature[21] as well as on graphene/Pt(111) surfaces at ~100−135 K.[14] The lattice constant of the experimentally observed bilayer ice is 0.481 nm,[14] which is in excellent agreement with that in the present work (0.482 nm).

Despite sharing an overall high structural similarity with the previously reported bilayer ice, close inspection of the system snapshot suggests that the bilayer ice nanodisc is not homogeneous in the x−y plane, because it contains many short-lived defects in the edge (bottom panel in Figure 3b). In other words, unlike the hexagonal arrangement of water in the central region, water molecules near the edge frequently switch

DOI: 10.1021/acs.jpclett.9b02512
J. Phys. Chem. Lett. 2019, 10, 6316−6323

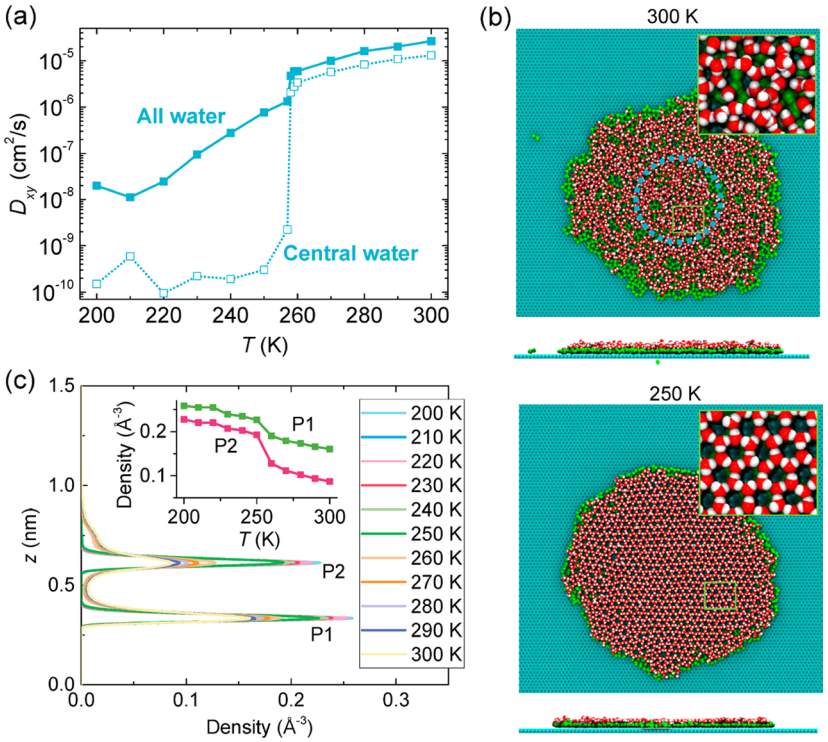

Figure 3. Freezing of water adlayers on a completely wetted solid surface (θ = 0). (a) Lateral diffusion coefficient of water D_{xy} as a function of gradually decreasing temperature T. Filled and empty squares correspond to D_{xy} for all molecules (termed "all water") and those within a 3 nm radius cylinder with its axis centered at the center of mass of the drop and normal to the surface (referred to as "central water", in the region circled in panel b), respectively. (b) Top (upper) and side (lower) views of a water disc at 300 K (top) and an ice disc at 250 K (bottom). The zoomed-in area shown in the top right corner is marked by a rectangular box. Water molecules inside the bottom and top water planes are shown as green and red particles, respectively. (c) Transverse density profiles of water oxygen atoms normal to the surface at different T. The inset shows the intensity of density peaks, P1 and P2, as a function of T.

their configurations between pentagons, heptagons, and other instant irregular hydrogen-boned networks, thus retaining a certain degree of mobility. In addition, we plotted in Figure 3a also D_{xy} but calculated solely based on water molecules in the central region (i.e., within a dotted circle in the top panel of Figure 3b) and found that the reduction in D_{xy} for central water (empty squares) at the freezing temperature is more than 2 orders of magnitude higher than that based on all water (filled squares). This result is in support of the nature of a strong first-order phase transition occurring in the central region of the disc.

Figure 3c shows the transverse oxygen density profiles under various T, which all display two evident peaks and manifest the two-layer nature of the water/ice. Two striking features can be seen in these profiles. On one hand, the intensities (or heights) of two peaks (namely P1 and P2) of the bilayer in the liquid state ($T \geq 260$ K) suddenly increase after freezing into the solid state ($T \leq 250$ K), confirming the first-order phase transition (inset of Figure 3c). This observation is again in line with previously reported confined bilayer water/ice.[15,16] On the other hand, under a given T, the two water planes of the present bilayer ice are not identical, because the two density peaks P1 and P2 differ from each other in terms of intensity and width. Note that previous confined bilayer ice consisted of two almost identical water planes.[15,16] This is because only a single solid surface is placed beneath the bottom water plane, unlike previous confined systems between two surfaces, thus breaking the symmetry of the present system along the direction perpendicular to the surface.

In the case of a strongly hydrophilic but not completely wetted surface (with a mild contact angle θ of 21.9°), the determined diffusion coefficients drop again upon cooling, at T between 252 and 251 K (Figure 4a). The resulting freezing/melting point is 251.5 K, which is 6.0 K lower than that on the completely wetted surface (257.5 K). To our surprise, the water drop seen at high temperatures (top inset in Figure 4a) does not freeze into an ice drop but instead further wets the surface and rapidly (within 50 ns) transforms into an ice disc (bottom inset in Figure 4a). The temporal evolution of this unexpected transition process is sketched in Figure S3. The structural difference between the two phases can also be reflected in density profiles (Figure 4b). The flat subsection in density curves distant from the solid surface exists at $T \geq 260$ K, corresponding to the presence of a liquid water drop; the flat subsection disappears at $T \leq 250$ K, manifesting the transition into a disc in a bilayer ice phase. Again, the abrupt increase in the density peak intensity (inset in Figure 4b) and reduction the diffusion coefficient (Figure 4a) on cooling suggest the first-order nature of the phase transition. A slight increase in θ to 29.2° retains the trend of phase transition but at a temperature of 237.5 K, which is 14 K lower than that on the surface with θ of 21.9°. Such a further-wetting process was also seen in previous MD simulations of a water droplet on hydrophilic surfaces, whereby a decrease in temperature resulted in further spreading of a water drop into a coexisting configuration of water drop and bilayer ice.[24]

Our discussion presented above has related the phase behavior of interfacial nanoscale water to the wettability of a surface. Indeed, it is known that, apart from the wettability,

DOI: 10.1021/acs.jpclett.9b02512
J. Phys. Chem. Lett. 2019, 10, 6316−6323

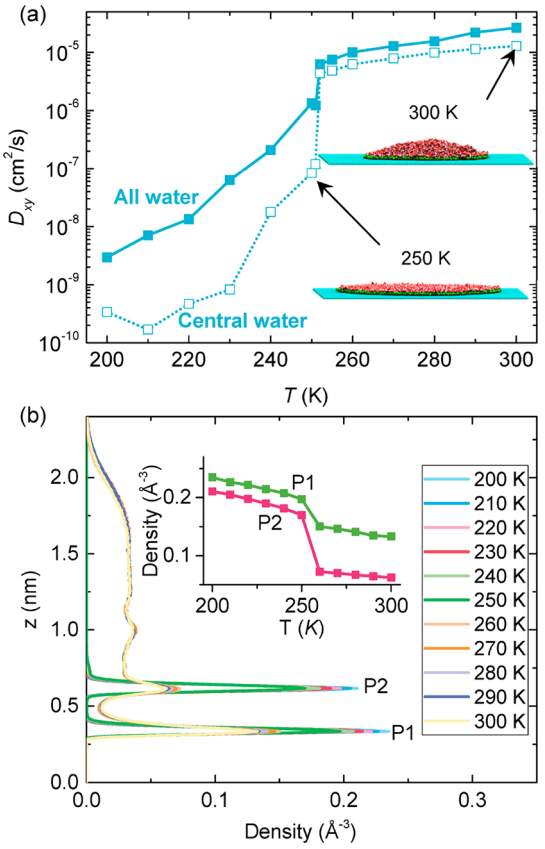

Figure 4. Freezing of a water drop into an ice disc on a hydrophilic surface with a contact angle θ of 21.9°. (a) Lateral diffusion coefficient of D_{xy} for all water (filled squares) and central water (empty squares) as a function of gradually decreasing temperature T. Insets show snapshots of a water nanodrop at 300 K and an ice nanodisc at 250 K. (b) Transverse density profiles of water oxygen atoms normal to the surface under different T. The inset shows density peak intensities as a function of T.

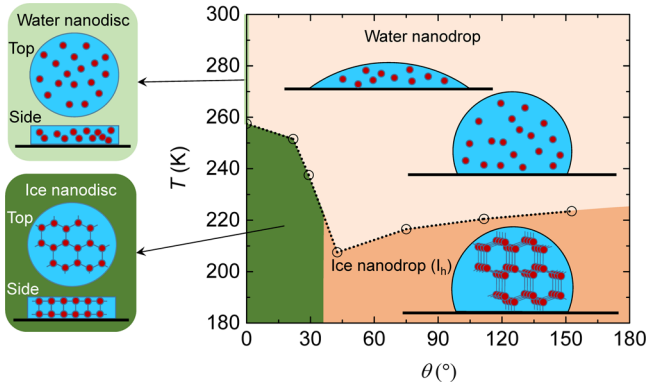

Figure 5. Schematic phase diagram of nanoscale water on surfaces at the wettability versus temperature (θ–T) plane. Each system contains 5665 water molecules. The vertical light green line indicates the phase of a water nanodisc on a completely wetted surface (i.e., θ = 0). Note that molecular configurations of different water and ice phases are not to scale.

other surface properties such as chemical composition and microscopic structures may also impact the interfacial water behavior. Therefore, we do not expect that the insight gained based on the present model surface can be used to unify the description of phase behavior on all kinds of solid substrates in general. For instance, a recent atomistic simulation study reported that an atomically flat graphite surface promoted heterogeneous nucleation of ice, while a molecularly rough surface with the same hydrophobicity did not.[30] On the other hand, the first contact layer of water/ice near different metal surfaces resolved at cryogenic temperatures (below about 200 K) in ultrahigh vacuum conditions, which usually tend to be hydrophilic, may contain various structures of water molecules including pentagons, hexagons, heptagons as well as their mixture, depending on the surface geometry.[2] In particular, instead of forming a complete hydrogen-bonded network, water molecules in the first contact layer could even be partially dissociated.[31] Very recently, Zhu carefully examined the formation of bilayer ice on various model fcc-crystal surface with indices of (100), (110), and (111) near room temperature and found that the liquid-to-bilayer ice transition depends on both water–surface interaction (or surface wettability) and surface structures.[32] In the present work, a model surface with the same geometry was employed in all cases to ensure the exploration of the wettability effect on water phase behaviors while neglecting other factors. Nevertheless, we saw evidence for the influence of surface geometry on interfacial water/ice phases. For instance, the ice disc is rotationally aligned with the surface lattice (bottom panel of Figure 3b), in line with experimental observations of two-layer ice on graphene.[14] To test whether the hexagonal bilayer ice was templated by the hexagonal arrangement of the model surface, we performed a series of MD simulations with a smooth (unstructured) and completely wetted surface and obtained again a similar hexagonal bilayer phase (Figure S4), albeit with a few pentagonal and heptagonal defects.

In summary, we have investigated the phase transition behavior of nanoscale water droplets/adlayers on surfaces with different wettabilities by using extensive MD simulations. The resulting schematic phase diagram in the wettability–temperature plane is sketched in Figure 5. Water drops on surfaces with contact angles of 42.6° or above freeze into ice drops containing ordinary hexagonal ice I_h at low temperatures. By contrast, a water disc on a completely wetted surface undergoes a water-to-ice freezing transition into a hexagonal ice bilayer. On surfaces with a mild contact angle (e.g., 21.9° and 29.2°), the stable liquid drop further wets the surface upon cooling and freezes into an ice disc. The present findings provide a comprehensive picture for phase behaviors of nanoscale interfacial water and have implications in applications ranging from catalysis to lubrication.

MODELS AND METHODS

Model Construction. We studied the phase behavior of a water nanodroplet (containing 5665 molecules, originally in a cubic box) placed on a model graphene-like plate (namely, atoms were arranged in a hexagonal lattice). Periodic boundary conditions were applied in the x–y direction, such that the plate was infinite. The plate size in the simulation cell was 24.10 × 24.28 nm^2 or 12.30 × 12.35 nm^3, chosen to allow for the formation of isolated water/ice nanodrops or nanodiscs in all cases. In the direct coexistence simulations of water nanodroplets for determination of the freezing/melting point, a I_h ice crystal tailored to spherical or cylindrical shape was used (as the seed), replacing some central water molecules in corresponding supercooled phases (e.g., Figure S2a). We

DOI: 10.1021/acs.jpclett.9b02512
J. Phys. Chem. Lett. 2019, 10, 6316–6323

preferred to use a spherical seed in all systems, with the largest possible diameter allowing to be placed in each water droplet. With this rule, the ice seeds used for water droplets on surfaces with contact angles of 152.8°, 111.6°, and 75.0° contained 3489, 2020, and 1031 water molecules, respectively (Figure S2b). These three systems with decreasing contact angles yielded a decreasing trend in the freezing/melting temperature (223.5, 220.5, and 210.5 K). However, on the surface with a further reduced contact angle of 42.6°, a very small spherical seed would be allowed if following this rule, and therefore, we used a cylindrical seed instead which contained 3150 water molecules. It is interesting to find that this system yields a freezing/melting temperature (207.5 K) following the above decreasing trend.

It has been noted that factors such as system and seed sizes, stochastic nature, and initial configuration could slightly influence the determined melting point.[33] Likewise, we found that the use of a smaller spherical seed for the droplet on a surface with a contact angle of 111.6° yielded a lower freezing/melting temperature (at 216.5 K, Figure S5b) than that of a larger seed (at 220.5 K, Figure S5a), while the change in seed shape from spherical to cubic but retaining the number of waters did not affect the freezing behavior (at 220.5 K, Figure S5c). We also performed a series of simulations for a much larger water droplet containing 15 945 water molecules on a surface with a contact angle of 111.6° (Figure S5d) and found an increased coexistence temperature at 229.5 K (compared to 220.5 K for the system of ∼5665 water molecules). This result indicates a size effect in affecting the freezing/melting temperature of the nanoscale water in the present work. Undoubtedly, the high-precision determination of the boundary between adjacent phases on substrates with various wettabilities is an important issue that deserves further study, using other effective methods, such as the one described by Lupi et al. based on the coarse grained model of water mW.[30] Furthermore, in a series of independent simulations, an unstructured and smooth wall was used to test the dependence of the present results on the atomic structure of the surface.

Simulations. Water molecules were described by the TIP4P/2005 water model.[27] Our test simulations via coexistence of a solid−liquid interface (with a simulation box containing liquid water and solid ice in contact) yielded the melting point of bulk I_h at 250.5 K (Figure S6), identical to the recommended value of this model.[28] Indeed, this melting point is ∼22.5 K lower than the experimental value of 273 K. Therefore, the phase transition temperature resolved in the present study should have been shifted to some extent. Despite this deficiency, the TIP4P/2005 water model was recognized as one of the best-performing nanopolarizable water models in describing the phase diagram of water, densities for different solid phases, as well as other thermodynamic and transport properties.[34] The interaction between atoms in the plate and water was modeled by the 12−6 Lennard-Jones (L-J) potential with the parameter σ_{O-Wall} = 0.335 nm. The other L-J parameter ε_{O-Wall} was adjusted over a range between 0.100 and 0.800 kJ/mol to model surfaces with various wettabilities. A similar strategy has been extensively used in previous studies.[24,35] In realistic experiments, the surface wettability could be varied by choosing different surface types (such as metals, metal oxides, and mica) or tuning surface microstructures. In addition, the wettability of a surface can be modulated over a wide range by coating self-assembled monolayers with customized terminal functional groups (such as −OH and $-CONH_2$).[4,5,36] On these surfaces the reorientation of interfacial water molecules due to water−functional group interactions as well as the surface flatness may impact the microscopic structures of interfacial water and associated phase behaviors depicted here. In the present work, we chose to tune wettability through a single parameter (ε_{O-Wall}), without altering surface geometry or functionalization, so as to focus on the effect of wettability on interfacial water behavior. For the unstructured wall, we opted for the 10−4 L-J potential for the water−wall interaction, with the same parameters as for the explicit wall but integrated over an infinitely large two-dimensional surface.

All MD simulations were performed with Gromacs 2016.4[37] and visualized with VMD.[38] A time step of 2 fs was used. The particle-mesh Ewald (PME) method was used to treat long-range electrostatics.[39] After energy minimization, all systems were first relaxed as the *NVT* ensemble (constant number of particles *N*, volume *V*, and temperature *T*) in simulations at 300 K for 50 ns. Subsequently, each system was gradually cooled with a temperature interval of 10 K, except at temperatures around the freezing/melting point where the interval was reduced to 1 or 2 K. The length of these simulations ranged from 50 ns to 2.1 μs, depending on the surface wettability and temperature. The Berendsen algorithm[40] to control the temperature was employed in most equilibration simulations to enable a quick relaxation, and additional test simulations with the Nosé−Hoover thermostat yielded qualitatively similar phase behaviors.

Calculation of Diffusion Coefficient. We traced each water molecule in the system that moved from position $\mathbf{r}(t)$ to $\mathbf{r}(t + \Delta t)$ within a given time interval Δt and computed its mean square displacement (MSD). The diffusion coefficient D was determined using Einstein's relation

$$\mathrm{MSD}(\Delta t) = \langle |\mathbf{r}(t + \Delta t) - \mathbf{r}(t)|^2 \rangle = 2nD\Delta t \quad (1)$$

where $\langle \cdots \rangle$ means the average over all waters and n is the number of dimensions in which the diffusion is considered. Computation of diffusion coefficient D in three dimensions adopts $n = 3$ while computation of lateral diffusion coefficient D_{xy} (in the x−y plane and parallel to the surface) adopts $n = 2$. $\mathrm{MSD}(\Delta t)$ was averaged over all pairs of trajectory frames that were separated by Δt.

Contact Angle Measurement. We performed a series of independent MD simulations to determine water contact angles on solid surfaces at different ε_{O-Wall} values. A slab geometry of the system was adopted (Figure S1), with a width of 3.197 nm (x direction) and a length (y direction) of 24.282 nm. Periodic boundary conditions were applied in all spatial directions, such that the water droplet was infinite in the x direction. The location of the surface is denoted as $z = 0$. A cubic box of water was placed initially above each surface, which subsequently beads up on hydrophobic surfaces and gradually spreads on hydrophilic ones (see Figure 1).

The water density distribution in the y−z plane was obtained by dividing the system into square bins with side lengths of 0.05 nm and averaging the density in each bin over considered frames of MD trajectories. A contour line with a density half of that of bulk water was plotted in the water isochore profiles, defining the boundary between liquid and vapor, and a circular fit was used to fit these data points (red line in Figure S1b). Note that density data below 8 Å from the surface were excluded from the calculations to avoid the influence of water−surface interaction on density fluctuation,

DOI: 10.1021/acs.jpclett.9b02512
J. Phys. Chem. Lett. 2019, 10, 6316−6323

as done in previous studies.[41] The contact angle θ was obtained as the angle between the surface and the tangent of the fitted curve at the surface ($z = 0$ in Figure S1b).

The contact angle θ of a macroscopic droplet can be described by Young's equation

$$\cos\theta = \frac{\gamma_{sv} - \gamma_{sl}}{\gamma_{lv}} \quad (2)$$

where γ_{sl}, γ_{sv}, and γ_{lv} are the solid−liquid, solid−vapor, and liquid−vapor surface tensions, respectively. However, for small droplets, especially down to the nanoscale, the dependence of contact angle on the droplet size due to the influence of the line tension was noticed in earlier reports.[8,41] In this case, the relationship between the macroscopic contact angle θ_∞ (contact angle corresponding to an infinitely large water droplet) and computed microscopic contact angle θ can be described by the "modified" Young's equation

$$\cos\theta = \cos\theta_\infty - \frac{\tau}{\gamma_{lv} r_B} \quad (3)$$

where τ denotes the line tension and r_B is the radius of the contact line of droplet (related to the drop size). In order to elucidate the dependence of contact angle on drop size, nanodroplets containing different numbers of water molecules were considered, and the corresponding θ was calculated for each case with the methodology described above. Subsequently, the variations of calculated $\cos\theta$ as a function of $1/r_B$ were plotted in Figure S1c. A linear fit into each series of data was adopted, and θ_∞ was obtained by extending the fit to the limit of infinitely large droplets ($1/r_B$ approaches 0). In the present work, surfaces described using ε_{O-Wall} at 0.100, 0.300, 0.476, 0.600, 0.635, and 0.650 kJ/mol yielded macroscopic contact angles θ_∞ at 152.8°, 111.6°, 75.0°, 42.6°, 29.2°, and 21.9°, respectively. Note that water can completely wet the surface with a larger ε_{O-Wall} (e.g., 0.800 kJ/mol), yielding a contact angle of 0.

■ ASSOCIATED CONTENT

Supporting Information

The Supporting Information is available free of charge on the ACS Publications website at DOI: 10.1021/acs.jpclett.9b02512.

Supporting figures and discussion related to contact angle determination, ice growth in water drops and bulk systems, phase transition on a solid surface with a mild contact angle, and ice disc on a smooth and completely wetted surface (PDF)

■ AUTHOR INFORMATION

Corresponding Authors

*E-mail: qiuhu@nuaa.edu.cn.
*E-mail: wlguo@nuaa.edu.cn.

ORCID

Hu Qiu: 0000-0001-9733-3132
Wanlin Guo: 0000-0001-6665-6924

Notes

The authors declare no competing financial interest.

■ ACKNOWLEDGMENTS

This work was supported by National Natural Science Foundation of China (11772152 and 51535005) and Jiangsu Province (BK20180065), the Six Talent Peaks Project in Jiangsu Province (SWYY-024), the Research Fund of State Key Laboratory of Mechanics and Control of Mechanical Structures (MCMS-I-0418K01 and MCMS-I-0419K01), the Fundamental Research Funds for the Central Universities (NC2018001, NP2019301, and NJ2019002), and a project funded by the Priority Academic Program Development of Jiangsu Higher Education Institutions.

■ REFERENCES

(1) Levy, Y.; Onuchic, J. N. Water mediation in protein folding and molecular recognition. *Annu. Rev. Biophys. Biomol. Struct.* **2006**, *35*, 389−415.
(2) Carrasco, J.; Hodgson, A.; Michaelides, A. A molecular perspective of water at metal interfaces. *Nat. Mater.* **2012**, *11*, 667−674.
(3) Asay, D. B.; Kim, S. H. Evolution of the adsorbed water layer structure on silicon oxide at room temperature. *J. Phys. Chem. B* **2005**, *109*, 16760−3.
(4) Godawat, R.; Jamadagni, S. N.; Garde, S. Characterizing hydrophobicity of interfaces by using cavity formation, solute binding, and water correlations. *Proc. Natl. Acad. Sci. U. S. A.* **2009**, *106*, 15119−24.
(5) Jamadagni, S. N.; Godawat, R.; Garde, S. Hydrophobicity of proteins and interfaces: insights from density fluctuations. *Annu. Rev. Chem. Biomol. Eng.* **2011**, *2*, 147−71.
(6) Park, S.-H.; Sposito, G. Structure of Water Adsorbed on a Mica Surface. *Phys. Rev. Lett.* **2002**, *89*, 085501.
(7) Rafiee, J.; Mi, X.; Gullapalli, H.; Thomas, A. V.; Yavari, F.; Shi, Y.; Ajayan, P. M.; Koratkar, N. A. Wetting transparency of graphene. *Nat. Mater.* **2012**, *11*, 217−222.
(8) Shih, C.-J.; Wang, Q. H.; Lin, S.; Park, K.-C.; Jin, Z.; Strano, M. S.; Blankschtein, D. Breakdown in the Wetting Transparency of Graphene. *Phys. Rev. Lett.* **2012**, *109*, 176101.
(9) Raj, R.; Maroo, S. C.; Wang, E. N. Wettability of Graphene. *Nano Lett.* **2013**, *13*, 1509−1515.
(10) Feibelman, P. J. The first wetting layer on a solid. *Phys. Today* **2010**, *63*, 34−39.
(11) Michaelides, A.; Morgenstern, K. Ice nanoclusters at hydrophobic metal surfaces. *Nat. Mater.* **2007**, *6*, 597−601.
(12) Carrasco, J.; Michaelides, A.; Forster, M.; Haq, S.; Raval, R.; Hodgson, A. A one-dimensional ice structure built from pentagons. *Nat. Mater.* **2009**, *8*, 427−31.
(13) Nie, S.; Feibelman, P. J.; Bartelt, N. C.; Thürmer, K. Pentagons and Heptagons in the First Water Layer on Pt(111). *Phys. Rev. Lett.* **2010**, *105*, 026102.
(14) Kimmel, G. A.; Matthiesen, J.; Baer, M.; Mundy, C. J.; Petrik, N. G.; Smith, R. S.; Dohnálek, Z.; Kay, B. D. No Confinement Needed: Observation of a Metastable Hydrophobic Wetting Two-Layer Ice on Graphene. *J. Am. Chem. Soc.* **2009**, *131*, 12838−12844.
(15) Koga, K.; Zeng, X. C.; Tanaka, H. Freezing of Confined Water: A Bilayer Ice Phase in Hydrophobic Nanopores. *Phys. Rev. Lett.* **1997**, *79*, 5262−5265.
(16) Koga, K.; Tanaka, H.; Zeng, X. C. First-order transition in confined water between high-density liquid and low-density amorphous phases. *Nature* **2000**, *408*, 564−567.
(17) Qiu, H.; Zeng, X. C.; Guo, W. Water in Inhomogeneous Nanoconfinement: Coexistence of Multilayered Liquid and Transition to Ice Nanoribbons. *ACS Nano* **2015**, *9*, 9877−9884.
(18) Kimmel, G. A.; Petrik, N. G.; Dohnálek, Z.; Kay, B. D. Crystalline Ice Growth on Pt(111): Observation of a Hydrophobic Water Monolayer. *Phys. Rev. Lett.* **2005**, *95*, 166102.
(19) Wang, C.; Lu, H.; Wang, Z.; Xiu, P.; Zhou, B.; Zuo, G.; Wan, R.; Hu, J.; Fang, H. Stable Liquid Water Droplet on a Water Monolayer Formed at Room Temperature on Ionic Model Substrates. *Phys. Rev. Lett.* **2009**, *103*, 137801.

DOI: 10.1021/acs.jpclett.9b02512
J. Phys. Chem. Lett. 2019, 10, 6316−6323

(20) Wang, C.; Zhou, B.; Xiu, P.; Fang, H. Effect of Surface Morphology on the Ordered Water Layer at Room Temperature. *J. Phys. Chem. C* **2011**, *115*, 3018−3024.
(21) Bampoulis, P.; Teernstra, V. J.; Lohse, D.; Zandvliet, H. J. W.; Poelsema, B. Hydrophobic Ice Confined between Graphene and MoS2. *J. Phys. Chem. C* **2016**, *120*, 27079−27084.
(22) Li, K.; Xu, S.; Shi, W.; He, M.; Li, H.; Li, S.; Zhou, X.; Wang, J.; Song, Y. Investigating the effects of solid surfaces on ice nucleation. *Langmuir* **2012**, *28*, 10749−54.
(23) Zheng, Y.; Su, C.; Lu, J.; Loh, K. P. Room-temperature ice growth on graphite seeded by nano-graphene oxide. *Angew. Chem., Int. Ed.* **2013**, *52*, 8708−12.
(24) Liu, J.; Zhu, C.; Liu, K.; Jiang, Y.; Song, Y.; Francisco, J. S.; Zeng, X. C.; Wang, J. Distinct ice patterns on solid surfaces with various wettabilities. *Proc. Natl. Acad. Sci. U. S. A.* **2017**, *114*, 11285−11290.
(25) Yin, L.; Xia, Q.; Xue, J.; Yang, S.; Wang, Q.; Chen, Q. In situ investigation of ice formation on surfaces with representative wettability. *Appl. Surf. Sci.* **2010**, *256*, 6764−6769.
(26) Chaudhary, G.; Li, R. Freezing of water droplets on solid surfaces: An experimental and numerical study. *Exp. Therm. Fluid Sci.* **2014**, *57*, 86−93.
(27) Abascal, J. L.; Vega, C. A general purpose model for the condensed phases of water: TIP4P/2005. *J. Chem. Phys.* **2005**, *123*, 234505.
(28) García Fernández, R.; Abascal, J. L. F.; Vega, C. The melting point of ice Ih for common water models calculated from direct coexistence of the solid-liquid interface. *J. Chem. Phys.* **2006**, *124*, 144506.
(29) Slater, B.; Michaelides, A. Surface premelting of water ice. *Nat. Rev. Chem.* **2019**, *3*, 172−188.
(30) Lupi, L.; Hudait, A.; Molinero, V. Heterogeneous nucleation of ice on carbon surfaces. *J. Am. Chem. Soc.* **2014**, *136*, 3156−3164.
(31) Forster, M.; Raval, R.; Hodgson, A.; Carrasco, J.; Michaelides, A. c(2 × 2) water-hydroxyl layer on Cu(110): a wetting layer stabilized by Bjerrum defects. *Phys. Rev. Lett.* **2011**, *106*, 046103.
(32) Zhu, C.; Gao, Y.; Zhu, W.; Jiang, J.; Liu, J.; Wang, J.; Francisco, J. S.; Zeng, X. C. Direct observation of 2-dimensional ices on different surfaces near room temperature without confinement. *Proc. Natl. Acad. Sci. U. S. A.* **2019**, *116*, 16723.
(33) Conde, M. M.; Rovere, M.; Gallo, P. High precision determination of the melting points of water TIP4P/2005 and water TIP4P/Ice models by the direct coexistence technique. *J. Chem. Phys.* **2017**, *147*, 244506.
(34) Vega, C.; Abascal, J. L. F.; Conde, M. M.; Aragones, J. L. What ice can teach us about water interactions: a critical comparison of the performance of different water models. *Faraday Discuss.* **2009**, *141*, 251−276.
(35) Zhu, C.; Li, H.; Huang, Y.; Zeng, X. C.; Meng, S. Microscopic insight into surface wetting: relations between interfacial water structure and the underlying lattice constant. *Phys. Rev. Lett.* **2013**, *110*, 126101.
(36) James, M.; Darwish, T. A.; Ciampi, S.; Sylvester, S. O.; Zhang, Z.; Ng, A.; Gooding, J. J.; Hanley, T. L. Nanoscale condensation of water on self-assembled monolayers. *Soft Matter* **2011**, *7*, 5309.
(37) Abraham, M. J.; Murtola, T.; Schulz, R.; Páll, S.; Smith, J. C.; Hess, B.; Lindahl, E. GROMACS: High performance molecular simulations through multi-level parallelism from laptops to supercomputers. *SoftwareX* **2015**, *1*−*2*, 19−25.
(38) Humphrey, W.; Dalke, A.; Schulten, K. VMD: visual molecular dynamics. *J. Mol. Graphics* **1996**, *14*, 33−38.
(39) Essmann, U.; Perera, L.; Berkowitz, M. L.; Darden, T.; Lee, H.; Pedersen, L. G. A smooth particle mesh Ewald method. *J. Chem. Phys.* **1995**, *103*, 8577−8593.
(40) Berendsen, H. J. C.; Postma, J. P. M.; Gunsteren, W. F. v.; DiNola, A.; Haak, J. R. Molecular dynamics with coupling to an external bath. *J. Chem. Phys.* **1984**, *81*, 3684−3690.
(41) Werder, T.; Walther, J. H.; Jaffe, R. L.; Halicioglu, T.; Koumoutsakos, P. On the Water-Carbon Interaction for Use in Molecular Dynamics Simulations of Graphite and Carbon Nanotubes. *J. Phys. Chem. B* **2003**, *107*, 1345−1352.

DOI: 10.1021/acs.jpclett.9b02512
J. Phys. Chem. Lett. 2019, 10, 6316−6323